







Cite this: *RSC Adv.*, 2020, 10, 41883

# SiC mesoporous membranes for sulfuric acid decomposition at high temperatures in the iodine–sulfur process†

Xin Yu,  Qing Wang,  Hiroki Nagasawa,  Masakoto Kanezashi   
and Toshinori Tsuru \*

Inorganic microporous materials have shown promise for the fabrication of membranes with chemical stability and resistance to high temperatures. Silicon-carbide (SiC) has been widely studied due to its outstanding mechanical stability under high temperatures and its resistance to corrosion and oxidation. This study is the first to prepare mesoporous SiC membranes for use in sulphuric acid decomposition to achieve thermochemical water splitting in the iodine–sulfur process. Single-gas permeation was carried out to confirm the stability of this mesoporous membrane under exposure to steam and H<sub>2</sub>SO<sub>4</sub> vapor. Benefiting from the excellent chemical stability of the α-Al<sub>2</sub>O<sub>3</sub> membrane support and the SiC particle layer, the SiC membrane exhibited stable gas permeance without significant degradation under H<sub>2</sub>SO<sub>4</sub> vapor treatment at 600 °C. Additionally, with extraction, the membrane reactor exhibited an increased conversion from 25 to 41% for H<sub>2</sub>SO<sub>4</sub> decomposition at 600 °C. The high performance combined with outstanding stability under acidic conditions suggests the developed SiC membrane is a promising candidate for H<sub>2</sub>SO<sub>4</sub> decomposition in a catalytic membrane reactor.

Received 11th August 2020  
Accepted 6th November 2020

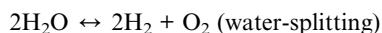
DOI: 10.1039/d0ra06919a

rsc.li/rsc-advances

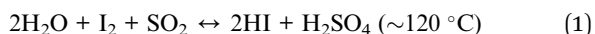
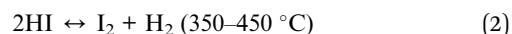
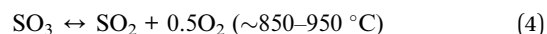
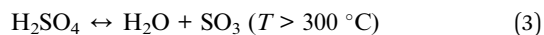
## 1. Introduction

Over the past twenty years, the water-splitting iodine–sulfur (IS) process has been extensively investigated as a sustainable technology with a net production of H<sub>2</sub> and O<sub>2</sub>, at much lower temperatures compared with the direct thermal decomposition of water.<sup>1–6</sup> The IS process involves cyclic reactions such as the Bunsen reaction and the thermal decompositions of sulfuric acid at 850–950 °C and hydroiodic acid at 450 °C. In these cycles, the decomposition of sulfuric acid requires temperatures so high that the heat of solar or nuclear energy must be utilized.<sup>3,5–7</sup>

Net reaction:



Bunsen reaction:


H<sub>2</sub> production:

O<sub>2</sub> production:


H<sub>2</sub>SO<sub>4</sub> decomposes to produce O<sub>2</sub> in the following two steps: H<sub>2</sub>SO<sub>4</sub> dissociates into H<sub>2</sub>O at 300 °C (eqn (3)) and sulfur trioxide (SO<sub>3</sub>), which further decomposes into sulfur dioxide (SO<sub>2</sub>) and oxygen (eqn (4)) *via* catalysis around 850 to 950 °C. O<sub>2</sub> production from H<sub>2</sub>SO<sub>4</sub> requires separation from co-produced SO<sub>2</sub>, SO<sub>3</sub> and H<sub>2</sub>O gaseous mixtures, while H<sub>2</sub> requires separation from HI and I<sub>2</sub>. H<sub>2</sub> and O<sub>2</sub> are collected *via* the separation process for further applications. The high temperature of SO<sub>3</sub> decomposition (>850 °C) can be lowered *via* equilibrium shift by extracting O<sub>2</sub> from the reaction systems. Membrane-based separation methods such as microfiltration,<sup>8</sup> ultrafiltration,<sup>9</sup> nanofiltration,<sup>10</sup> reverse osmosis,<sup>11</sup> and gas separation<sup>12</sup> consume the least amount of energy compared with other separation techniques.<sup>13</sup> Membrane processes also provide a significant, convenient, and sustainable solution for H<sub>2</sub> and O<sub>2</sub> separation.<sup>14–18</sup>

In recent years, several types of membranes have been developed for the iodine–sulfur cycle.<sup>4,19–28</sup> Myagmarjav *et al.* reported that a hexyltrimethoxysilane (HTMOS) derived silica membrane achieved H<sub>2</sub> permeance on the order of 10<sup>–7</sup> mol

Department of Chemical Engineering, Graduate School of Engineering, Hiroshima University, 1-4-1 Kagamiyama, Higashi-Hiroshima 739-8527, Japan. E-mail: tsuru@hiroshima-u.ac.jp

† Electronic supplementary information (ESI) available. See DOI: 10.1039/d0ra06919a



$\text{m}^{-2} \text{s}^{-1} \text{Pa}^{-1}$  with  $\text{H}_2/\text{HI}$  selectivity of more than 175.<sup>4</sup> In addition, their silica-based ceramic membrane reactor achieved HI conversion of 0.70 and  $\text{H}_2$  extraction of 0.98 at 400 °C.<sup>27</sup> However, it was also reported that silica membranes can't survive under humid environments at high temperatures,<sup>29</sup> and challenges remain for the use of silica membranes when using water in Bunsen reaction and  $\text{H}_2\text{SO}_4$  decomposition reaction. Nomura *et al.* proposed a cation exchange membrane (CEM) constructed from polymerized divinylbenzene on Nafion for Bunsen reaction.<sup>19</sup> HI and  $\text{H}_2\text{SO}_4$  were obtained separately from CEM-divided cells by feeding  $\text{SO}_2$ ,  $\text{I}_2$  and  $\text{H}_2\text{O}$ . He *et al.* discovered two Pt/carbon catalyst coated membranes (CCMs) that showed a reduced charge transfer resistance for the Bunsen reaction at room temperature.<sup>24</sup> The electrolytic voltage was reduced by 62.7% with cathode current efficiency that reached 97.41%. However, water permeated the cation exchange membrane to form  $\text{H}_2\text{SO}_4$ , and resistance to  $\text{H}_2\text{SO}_4$  remains unsolved. Several recent results have also shown promising membrane performances under  $\text{H}_2\text{SO}_4$  for the IS process. PTFE-based materials were reportedly stable even after exposure to highly concentrated  $\text{H}_2\text{SO}_4$  solutions at 80–120 °C.<sup>30</sup> Non-fluorinated membranes (*e.g.*, polybenzimidazole, non-fluorinated poly(arylene ether sulfone)) have also shown excellent stability against 30 and 60 wt%  $\text{H}_2\text{SO}_4$  at 80 °C.<sup>31</sup> However, for  $\text{O}_2$  separation in integrated  $\text{H}_2\text{SO}_4$  decomposition systems, stability under high temperatures (600–900 °C) for the second reaction, which is expressed as eqn (4), and for corrosion under strongly acidic conditions remains a challenge.

Generally, inorganic membranes are prepared with the strength to withstand high temperatures as well as oxidative and chemical conditions, which makes them promising candidates for  $\text{O}_2$  separation from  $\text{SO}_3$  decomposition, as mentioned in eqn (4). Notably, we reported several classes of inorganic membrane materials/metal oxides employed in membrane reactors for  $\text{O}_2/\text{SO}_3$  separation.<sup>3,5</sup>  $\text{SiO}_2$  membranes, due to their excellent thermal stability and high gas selectivity,<sup>17,32</sup> were first used by our team for  $\text{O}_2/\text{SO}_2$  separation in 2015.<sup>3</sup> Bis(triethoxysilyl)ethane (BTESE)-derived membranes, particularly those fabricated under high temperatures, have demonstrated high oxidation resistance and exhibited an  $\text{O}_2/\text{SO}_3$  selectivity of 10 with an  $\text{O}_2$  permeance of  $2.5 \times 10^{-8} \text{ mol m}^{-2} \text{s}^{-1} \text{Pa}^{-1}$ .<sup>33</sup> Despite a decrease in permeance after exposure to  $\text{SO}_3$ , the BTESE membrane exhibited a very high level of  $\text{SO}_3$  stability. On the other hand, highly water stable BTESE membranes have also been studied,<sup>17,34</sup> and these have served as selective filters for  $\text{H}_2\text{O}/\text{O}_2/\text{SO}_3$  separation. In addition, the membrane materials with high  $\text{SO}_3$  (10% in  $\text{O}_2$ ) resistance at 550 °C, such as  $\text{SiO}_2$ ,  $\text{SiO}_2\text{-ZrO}_2$  (high Si/Zr ratio), and  $\alpha\text{-Al}_2\text{O}_3$  powders were fundamentally studied.<sup>5</sup>

To the best of our knowledge, however, no study has yet reported the chemical stability of membrane materials against sulfuric acid at high temperatures (>400 °C), and as yet no effective strategy has been developed to fabricate an  $\text{O}_2$ -selective membrane structure. Moreover, there has been no report of an attempt to apply a membrane reactor to  $\text{H}_2\text{SO}_4$  decomposition. However, the use of high temperatures is essential for the separation of  $\text{O}_2$  through membrane and catalytic

decomposition of  $\text{H}_2\text{SO}_4$ . The present study expands our previous work on the stability of various types of metal oxides under  $\text{SO}_3$  exposure,<sup>5</sup> and provides insight from evaluating the characteristics of  $\text{SiO}_2$ ,  $\text{ZrO}_2$ , SiC, homemade  $\text{Al}_2\text{O}_3$ ,  $\text{SiO}_2\text{-ZrO}_2$ , and  $\alpha\text{-Al}_2\text{O}_3$  under  $\text{H}_2\text{SO}_4$  vapor at high temperatures. After clarifying the chemical stability, the  $\text{H}_2\text{SO}_4$  decomposition conversion of the membrane fabricated by SiC was further studied.

## 2. Experiments

### 2.1 Preparation of sol, gel and powders

$\text{SiO}_2\text{-ZrO}_2$  sols with sol concentrations of 2.0 wt% were synthesized from tetraethoxysilane (TEOS) and zirconium butoxide solutions (ZrBT, 80% in 1-butanol) in Si/Zr molar ratios of 5/5, 7/3 and 10/0 by hydrolysis and condensation reactions in  $\text{H}_2\text{O}$  with HCl (35 wt%) as the catalyst. The details can be found in our previous reports.<sup>5,35</sup>  $\text{Al}_2\text{O}_3$  gels were prepared *via* hydrolysis and condensation by mixing aluminium tri-*sec*-butoxide (AlTBT, 97%) with water, and HCl in molar ratios of AlTBT/ $\text{H}_2\text{O}$ /HCl = 1/10/0.1.  $\text{ZrO}_2$  sol was prepared *via* hydrolysis and condensation by mixing ZrBT,  $\text{H}_2\text{O}$ , and HCl in molar ratios of ZrBT/ $\text{H}_2\text{O}$ /HCl = 1/1/0.1. Ethanol (99.5%) was added to adjust the concentration of AlTBT or ZrBT sols at 5 wt%.  $\text{Al}_2\text{O}_3$ ,  $\text{SiO}_2$ ,  $\text{ZrO}_2$ , and  $\text{SiO}_2\text{-ZrO}_2$  powders were prepared by drying  $\text{Al}_2\text{O}_3$ ,  $\text{SiO}_2$ ,  $\text{ZrO}_2$ , and  $\text{SiO}_2\text{-ZrO}_2$  (Si/Zr ratio = 7/3) gels at 50 °C and subsequently calcined at 600 °C under air for 24 h.

### 2.2 Characterizations

After drying  $\text{SiO}_2$ ,  $\text{ZrO}_2$ , homemade  $\text{Al}_2\text{O}_3$ ,  $\text{SiO}_2\text{-ZrO}_2$  (Si/Zr ratio of 7/3), and SiC powders at 600 °C under air, the exposure experiment was carried out in a quartz cell in which these powders were exposed to either  $\text{H}_2\text{O}$  or  $\text{H}_2\text{SO}_4$  (98%) vapor under an absolute pressure of 1 bar at 600 °C for 24 h. Then, 2 ml of liquid ( $\text{H}_2\text{O}$  or  $\text{H}_2\text{SO}_4$ ) was added into the quartz tube before heating, and after heating at 600 °C, and the vaporized liquid was refluxed in the tube as schematically shown in the diagram in the Fig. S1.† Powders were also exposed with an  $\text{SO}_3$  of 10 kPa at 600 °C under sweep conditions similar to our previous report.<sup>5</sup> Subsequently, those powders were followed by drying at 500 °C under air to remove the adsorbed gas on the surface. Then, characterizations of powders were carried out using Energy Dispersive X-ray Spectroscopy (EDS) Scanning Electron Microscopy (SEM, JCM-5700, JEOL Ltd.), X-ray diffraction (XRD, Bruker AXS, Japan), and  $\text{N}_2$  adsorption under liquid nitrogen at 77 K (BELMAX, BEL Japan Inc.).

### 2.3 Preparation of mesoporous membranes

Fabrication of membranes for  $\text{H}_2\text{SO}_4$  separation,  $\alpha\text{-Al}_2\text{O}_3$  membrane support (cylindrical porous tubes with average pore size 2  $\mu\text{m}$ ; outer diameter 1 cm; length 10 cm, Nikkato. Corp.) were used as substrates. 5 types membranes were fabricated as shown in Table 1. The outer surfaces of the tube were coated with  $\alpha$ -alumina (2.0 and 0.2  $\mu\text{m}$ , Sumitomo Chemical Co., Ltd) or silicon carbide (2.3 and 0.5  $\mu\text{m}$ , Pacific Rundum Co., Ltd.) particles mixed with the sols ( $\text{SiO}_2\text{-ZrO}_2$  at Si/Zr ratio of 5/5, 7/3



**Table 1** Conditions of the membrane fabrication by using various particles and binder sols

No.	Particles	Binder sols
M1	—	—
M2	$\alpha$ -Al <sub>2</sub> O <sub>3</sub>	SiO <sub>2</sub> -ZrO <sub>2</sub> (5/5)
M3	$\alpha$ -Al <sub>2</sub> O <sub>3</sub>	SiO <sub>2</sub> -ZrO <sub>2</sub> (7/3)
M4	SiC	SiO <sub>2</sub> -ZrO <sub>2</sub> (7/3)
M5	SiC	SiO <sub>2</sub> -ZrO <sub>2</sub> (10/0)

or 10/0) as the binder to create a smooth and homogeneous surface, followed by firing at 600 °C for 15 min then cooling to room temperature. This procedure of coating particle layers was repeated several times to reduce the pore sizes of the membranes to approximately 20 nm. The schematic membrane structure is shown in Fig. 1.

## 2.4 Gas permeance of membranes and H<sub>2</sub>SO<sub>4</sub> conversion

The gas permeation of membranes during H<sub>2</sub>SO<sub>4</sub> and H<sub>2</sub>O exposure was tested in membrane module shown schematically in Fig. 2. Distilled H<sub>2</sub>O (0.48 ml h<sup>-1</sup>) or H<sub>2</sub>SO<sub>4</sub> (1.0 ml h<sup>-1</sup>) was introduced into the membrane *via* a syringe pump, and helium was supplied as a carrier gas (flow rate of 90 ml min<sup>-1</sup>) to control the molar ratio of H<sub>2</sub>O or H<sub>2</sub>SO<sub>4</sub> at 0.1 bar. Membranes of different types, M1–M5, were placed in an electric furnace with a controlled inner-side temperature of 600 °C for evaporation and reaction. Once H<sub>2</sub>SO<sub>4</sub> was injected inside the heated zone, liquid H<sub>2</sub>SO<sub>4</sub> was evaporated, and then thermally decomposed into sulfur trioxide and water vapor. After exposure tests for several hours, membranes were dried with N<sub>2</sub> flow in the furnace at 600 °C, followed by cooling to room temperature. Then, the membrane module and gas lines were carefully cleaned by water to wash out the remaining H<sub>2</sub>SO<sub>4</sub> and dried in an 80 °C oven. Pure gas permeance was measured under the transmembrane pressure difference from 0.01 to 1 bar by feeding gas to the outside of the membrane.

An M4 membrane was used for the membrane reactor to investigate the effect of O<sub>2</sub> extraction on H<sub>2</sub>SO<sub>4</sub> decomposition conversion. At 600 °C, the liquid sulphuric acid changes to a gas phase, and the decomposition reaction can be split into two

endothermic sub-reactions. The first sub-reaction is the dissociation of sulphuric acid into sulphur trioxide and water (reaction (3)), and the second is the decomposition of sulphur trioxide into sulphur dioxide and oxygen (reaction (4)). Here, SO<sub>3</sub> was decomposed to SO<sub>2</sub> with the Pt/Al<sub>2</sub>O<sub>3</sub> catalyst (1.5 g, Shimadzu Corporation), which was packed inside the membrane. Outlet gases from the membrane reactor, consisting of mixtures of carrier gas He, and H<sub>2</sub>O, SO<sub>3</sub>, SO<sub>2</sub>, and O<sub>2</sub>, as produced from H<sub>2</sub>SO<sub>4</sub> decomposition, subsequently passed through two bottles filled with 120 ml sodium hydroxide aqueous solution (20 wt%), where H<sub>2</sub>O was condensed and SO<sub>3</sub> or SO<sub>2</sub> was trapped by the neutralization reaction. So the outlet gas consisted of He and O<sub>2</sub> and was measured using a soap film bubble flowmeter. NaOH was chosen for acidic gas absorption because it had high efficiency (nearly 100%) with SO<sub>2</sub> removal.<sup>36</sup> For safety, a SO<sub>2</sub> alarm (ToxiRAE II, PGM-1130) was set nearby the equipment to signal SO<sub>2</sub> leakage, and the outlet gas in the NaOH trap was monitored by the SO<sub>2</sub> alarm and the SO<sub>2</sub> content was found to be lower than 1 ppm.

H<sub>2</sub>SO<sub>4</sub> conversion (*w*) can be quantified by the ratio of produced O<sub>2</sub> over theoretical O<sub>2</sub> since 1 mol of H<sub>2</sub>SO<sub>4</sub> can produce 0.5 mol of O<sub>2</sub> after complete conversion. Therefore, the conversion can be expressed in the following equation:

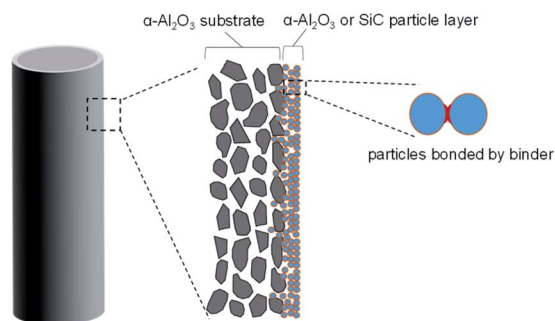
$$w = \frac{F_r + F_p - F_c}{0.5F_h} \times 100\%$$

In that equation, *F<sub>r</sub>* and *F<sub>p</sub>* are the gas molar rate (mol s<sup>-1</sup>) of retentate and permeate side of the membrane, *F<sub>c</sub>* is the molar rate of carried gas He. *F<sub>h</sub>* (mol s<sup>-1</sup>) is the feed rate of liquid H<sub>2</sub>SO<sub>4</sub>. It is of note that H<sub>2</sub>SO<sub>4</sub> was 100% decomposed to H<sub>2</sub>O and SO<sub>3</sub> at 450 °C, hence, from this perspective, the H<sub>2</sub>SO<sub>4</sub> conversion to SO<sub>2</sub> was dominated by SO<sub>3</sub> decomposition.

## 3. Results and discussion

### 3.1 Stability of membrane materials under H<sub>2</sub>SO<sub>4</sub> exposure

It has been pointed out that the  $\alpha$ -Al<sub>2</sub>O<sub>3</sub>, SiO<sub>2</sub> and lower-Zr-content SiO<sub>2</sub>-ZrO<sub>2</sub> powders had good chemical stability against SO<sub>2</sub> and SO<sub>3</sub> even at 550 °C for O<sub>2</sub>/SO<sub>2</sub> or O<sub>2</sub>/SO<sub>3</sub> separation.<sup>5,37</sup> The H<sub>2</sub>SO<sub>4</sub> decomposition generates water vapor at temperatures higher than 300 °C, and, hence, the stability and corrosion under steam/acid still needs to be addressed. Therefore, Fig. 3 depicts the XRD patterns of the samples after being treated in SO<sub>3</sub> or H<sub>2</sub>SO<sub>4</sub> vapor at 600 °C for 24 h. The XRD patterns of SiO<sub>2</sub> (Fig. 3A) showed a broad single peak centered at 23°, which was assigned to an amorphous SiO<sub>2</sub> phase, and no other peaks were observed in the XRD patterns. Additionally, Nadar *et al.* also reported that TG-DTA and XRD patterns of SiO<sub>2</sub> after H<sub>2</sub>SO<sub>4</sub> exposure were similar to those before H<sub>2</sub>SO<sub>4</sub>,<sup>38</sup> indicating the high acid resistance of SiO<sub>2</sub>. Table 2 shows the BET area of SiO<sub>2</sub> powders was largely decreased after being treated in steam and in H<sub>2</sub>SO<sub>4</sub> vapor. The reason for this decrease in the BET area could have centered around the reaction of Si–O–Si and H<sub>2</sub>O to form Si–OH, which could have led to large non-selective pores and resultant particles that became dense.<sup>34,39</sup> XRD analyses of  $\alpha$ -Al<sub>2</sub>O<sub>3</sub> (Fig. 3B) powders revealed that the S in Al<sub>2</sub>(SO<sub>4</sub>)<sub>3</sub> and the percentage of sulfur/aluminum

**Fig. 1** The schematic structure of  $\alpha$ -Al<sub>2</sub>O<sub>3</sub> or SiC particle membranes.

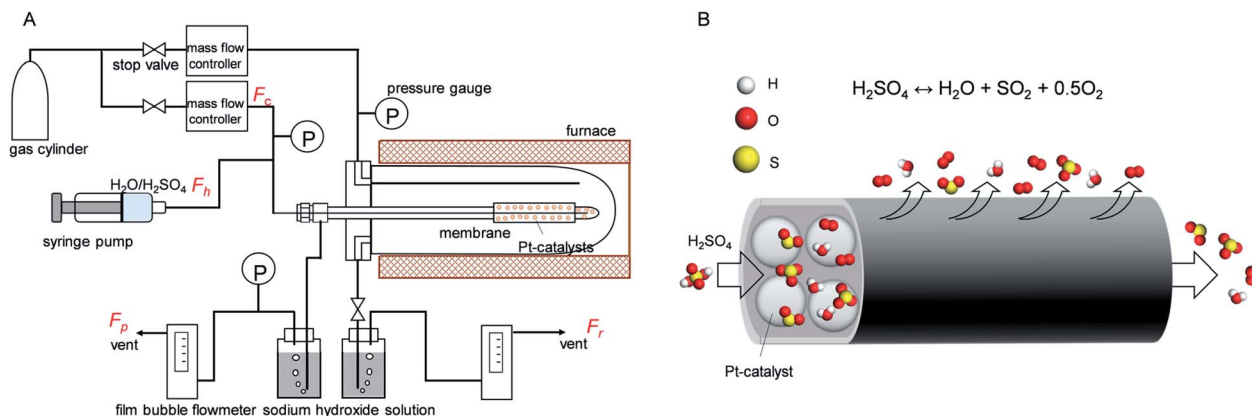


Fig. 2 (A) Schematic diagram of the experiment for steam and sulphuric acid treatment and gas permeance measurement. (B) Schematic illustration of the SiC membrane used membrane reactor for  $H_2SO_4$  decomposition.

detected by EDS had increased from 0.87 to 26%, as shown in Table 2. Also, the FT-IR spectra confirmed that an  $SO_4$  peak was formed in  $\alpha-Al_2O_3$  (ESI-2<sup>†</sup>), which was attributed to the reaction of alumina with the  $H_2SO_4$  vapor at 600 °C. Furthermore, BET analyses revealed how the surface area of  $\alpha-Al_2O_3$  had decreased from 8.8 to 1.9  $m^2 g^{-1}$  following exposure to  $H_2SO_4$ , presumably due to the formation of  $Al_2(SO_4)_3$  on the surface, which reduced the size of the pores. Regarding the homemade  $Al_2O_3$  powder, which had a high surface area of 226  $m^2 g^{-1}$  compared with that

of crystalline  $\alpha-Al_2O_3$  at 8.8  $m^2 g^{-1}$ , the BET area was drastically decreased after exposure to  $SO_3$  and  $H_2SO_4$ , but the reactivity was significantly greater under  $H_2SO_4$  vapor than under  $SO_3$ . Fig. 3C shows the XRD of  $ZrO_2$ , which exhibited an increased crystalline monoclinic (m)  $ZrO_2$  from the tetragonal (t) phase<sup>40</sup> due to the temperature swings of the membrane furnace and the dryer oven. XRD analysis did not detect the sulfate phase for  $ZrO_2$  and  $SiO_2-ZrO_2$  (Si/Zr = 7/3) powders after  $SO_3$  exposure, as shown in Fig. 3C and D, and corresponded to low S ratios of 2.7

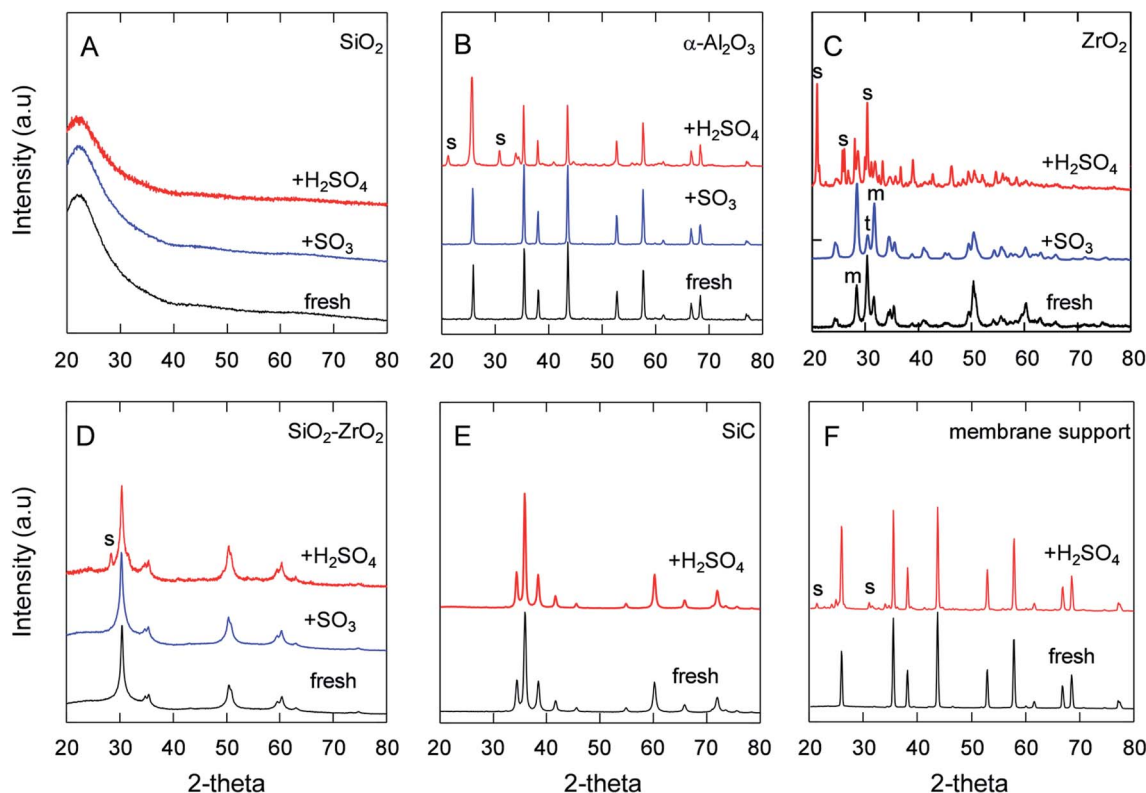


Fig. 3 XRD of different powders after  $SO_3$  or  $H_2SO_4$  exposure at 600 °C under one-atmosphere pressure. S: zirconium sulfate or aluminum sulfate, t/m: tetragonal/monoclinic  $ZrO_2$ . (A) Home-made  $SiO_2$ . (B)  $\alpha-Al_2O_3$ . (C)  $ZrO_2$ . (D)  $SiO_2-ZrO_2$  (Si/Zr = 7/3). (E) SiC. (F)  $\alpha-Al_2O_3$  membrane support.





Table 2 BET area and S ratio of powders after H<sub>2</sub>O or H<sub>2</sub>SO<sub>4</sub> exposure

Powders	Air-fired temperature (°C)	BET area (m <sup>2</sup> g <sup>-1</sup> )			S/Al or S/(Si + Zr) mole ratio (%)
		Fresh	After H <sub>2</sub> O	After H <sub>2</sub> SO <sub>4</sub>	
SiO <sub>2</sub>	600	650	600	390	<0.1
Home-made Al <sub>2</sub> O <sub>3</sub>	600	226	18	6.4	86
α-Al <sub>2</sub> O <sub>3</sub>	>1200	8.8	11	1.9	26
Membrane support	>1200	0.21	0.14	0.57	17
SiO <sub>2</sub> -ZrO <sub>2</sub>	600	115	25	14.9	4.0
ZrO <sub>2</sub>	600	21	20	3.2	100
SiC	>1800	10.0	10.5	9.0	<0.1

and 2.2%,<sup>5</sup> respectively. On the contrary, after exposure to H<sub>2</sub>SO<sub>4</sub> vapor at the same temperature of 600 °C, the S ratio was quite different between ZrO<sub>2</sub> and SiO<sub>2</sub>-ZrO<sub>2</sub> powders. The XRD spectra in Fig. 3C shows the formation of Zr(SO<sub>4</sub>)<sub>2</sub> from ZrO<sub>2</sub> after H<sub>2</sub>SO<sub>4</sub> exposure, with only a small amount of crystalline Zr(SO<sub>4</sub>)<sub>2</sub> (S peak)<sup>41</sup> detected for SiO<sub>2</sub>-ZrO<sub>2</sub> (Fig. 3D). In addition, Table 2 shows the S content measured by EDS was almost 100 and 4.0% for ZrO<sub>2</sub> and SiO<sub>2</sub>-ZrO<sub>2</sub> powders, respectively. Probable reasons for the high sulfur composition in ZrO<sub>2</sub> powders after exposure to H<sub>2</sub>SO<sub>4</sub> vapor could be primarily that H<sub>2</sub>O activated ZrO<sub>2</sub> and formed ZrO(OH)<sub>2</sub> or Zr(OH)<sub>4</sub> at high temperature.<sup>42</sup> Another explanation could be that either ZrO(OH)<sub>2</sub> or Zr(OH)<sub>4</sub> was more active in the reaction with SO<sub>3</sub> to form Zr(SO<sub>4</sub>)<sub>2</sub>. Fig. 3E shows the XRD spectra of silicon-carbide powders before and after H<sub>2</sub>SO<sub>4</sub> exposure. No change in peaks was observed, probably because SiC is generally known for its ultrahigh chemical and thermal stability.<sup>43–45</sup> Additionally, the α-Al<sub>2</sub>O<sub>3</sub> membrane supports used in this study were proven to be chemically stable under H<sub>2</sub>SO<sub>4</sub>, which was confirmed by XRD analysis to have a lesser amount of aluminum sulfate (Fig. 3F) compared with that of α-Al<sub>2</sub>O<sub>3</sub> powders (Fig. 3B). This was probably because SiO<sub>2</sub> was added to the Al<sub>2</sub>O<sub>3</sub> membrane supports since Si was detected in the Al<sub>2</sub>O<sub>3</sub> membrane supports, although the exact content was not available. Although the S content was 17% for α-Al<sub>2</sub>O<sub>3</sub> membrane supports after H<sub>2</sub>SO<sub>4</sub> exposure, the change in the element composition of the substrates had less of an effect on gas permeation (Fig. 5). To benefit the stability of these materials against H<sub>2</sub>SO<sub>4</sub> in the IS

process, the use of α-Al<sub>2</sub>O<sub>3</sub> membrane supports, SiC and SiO<sub>2</sub>-ZrO<sub>2</sub> were proposed for the preparation of SiC membranes.

Fig. 4 features the SEM micrographs of SiO<sub>2</sub>, α-Al<sub>2</sub>O<sub>3</sub> and ZrO<sub>2</sub> before and after exposure to H<sub>2</sub>SO<sub>4</sub>. As shown in the images of Fig. 4A1 and A2, the surface of SiO<sub>2</sub> powders were smooth after H<sub>2</sub>SO<sub>4</sub> exposure, which demonstrated morphological differences between the fresh state and after SO<sub>3</sub> exposure<sup>5</sup> while maintaining approximately the same particle size. This could be explained by the densification of SiO<sub>2</sub> fine particles induced by the reaction between Si-O-Si and H<sub>2</sub>O. Fig. 4B1 and B2 shows that α-Al<sub>2</sub>O<sub>3</sub> particles had a relatively uniform morphology even after H<sub>2</sub>SO<sub>4</sub> exposure while the size of the Al<sub>2</sub>O<sub>3</sub> particles grew larger due to the formation of low-melting Al<sub>2</sub>(SO<sub>4</sub>)<sub>3</sub> on the surface, with which each of the primary particles seemed to be connected and aggregated that differed from the α-Al<sub>2</sub>O<sub>3</sub> particles with SO<sub>3</sub> exposure.<sup>5</sup> Given that α-Al<sub>2</sub>O<sub>3</sub> particles after exposure were deposited with, and covered by, the Al<sub>2</sub>(SO<sub>4</sub>)<sub>3</sub>, these SEM photos confirm the compositions obtained by EDS. The SEM images in Fig. 4C1 and C2 also show that the fine ZrO<sub>2</sub> particles had reacted with the H<sub>2</sub>SO<sub>4</sub> vapor and increased in size, which is similar to the growth of α-Al<sub>2</sub>O<sub>3</sub> powder under H<sub>2</sub>SO<sub>4</sub> exposure, probably due to the effect of dissolution under the H<sub>2</sub>O vapor and to the reaction with SO<sub>3</sub>.

### 3.2 Permeance of the SiC membrane reactor for H<sub>2</sub>SO<sub>4</sub> decomposition

Porous inorganic membranes were first explored under an extreme condition, *i.e.*, H<sub>2</sub>SO<sub>4</sub> decomposition at 600 °C. Fig. 5

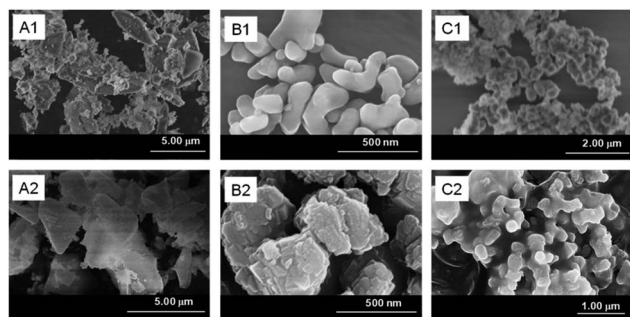


Fig. 4 SEM of fresh SiO<sub>2</sub> (A1), α-Al<sub>2</sub>O<sub>3</sub> (B1), ZrO<sub>2</sub> (C1) powders. (A2), (B2) and (C2) were those powders after H<sub>2</sub>SO<sub>4</sub> (100 kPa) exposure at 600 °C, respectively.

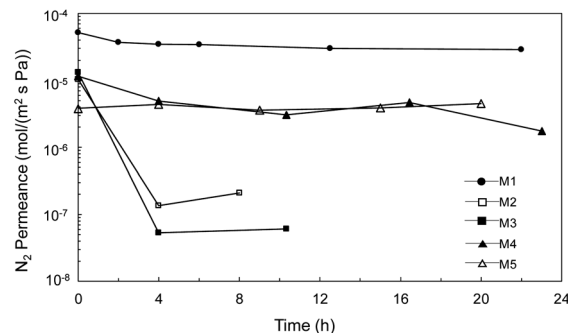


Fig. 5 Time course of N<sub>2</sub> permeance for α-Al<sub>2</sub>O<sub>3</sub> membrane support (M1) and membrane prepared by Al<sub>2</sub>O<sub>3</sub> particle layer (M2, M3), and SiC particle (M4, M5) after the treatment under H<sub>2</sub>SO<sub>4</sub> vapor at 600 °C.



shows the time course of the  $N_2$  permeance with increases in the treatment time under  $H_2SO_4$  vapor. The  $N_2$  permeance of the  $\alpha-Al_2O_3$  membrane support (M1) was decreased only slightly even after 22 h of exposure to  $H_2SO_4$  vapor at 600 °C, since the membrane support provided only moderate chemical stability, as shown in Fig. 3F (XRD) and Table 2, and the large pores changed very little even after sulfate formation. M2, M3, and M4 prepared with different particles (SiC,  $\alpha-Al_2O_3$ ) and binders ( $SiO_2-ZrO_2$ ,  $SiO_2$ ) showed  $N_2$  permeance at the same level ( $10^{-5} \text{ mol m}^{-2} \text{ s}^{-1} \text{ Pa}^{-1}$ ) as before the stability test, which provided a fair comparison and verified good reproducibility of the membrane fabrication. Values were drastically decreased for the permeance of both M2 and M3  $Al_2O_3$  particle layers following  $H_2SO_4$  exposure for 4 h. The permeance of M2 was further decreased, however, confirming that the high Zr content in the binder (Si/Zr = 5/5) was more unstable due to the formation of  $Zr(SO_4)_2$  with  $H_2SO_4$ , similar to high Zr content  $SiO_2-ZrO_2$  (Si/Zr = 5/5) in  $SO_3$ .<sup>5</sup> These results were reasonable, and strongly suggested that the membranes should be prepared using Si-rich  $SiO_2-ZrO_2$  (Si/Zr = 7/3) as a binder. M4 and M5 SiC particle layers showed a very small decrease and high relative permeance over all the particle membranes, M2–M5. That indicated that the membrane prepared by SiC with Si-rich  $SiO_2-ZrO_2$  (Si/Zr = 7/3) increased both the chemical and hydrothermal stability compared with that of the  $Al_2O_3$  particle layers with Zr-rich  $SiO_2-ZrO_2$  used to fabricate M2 and M3. The morphology changed less for membranes fabricated with SiC layers following exposure to  $H_2SO_4$  (ESI-3†), which corresponds to the stability confirmed by XRD and BET results. These results suggested that the SiC was stable for fabricating a particle layer for membrane preparation in the IS process.

Catalytic membrane reactor for  $H_2SO_4$  decomposition, liquid  $H_2SO_4$  (98%) was fed at a flow rate of  $1.0 \text{ ml h}^{-1}$  and He was used as the carrier gas with a flow rate of  $24.5 \text{ ml min}^{-1}$  controlled by a mass flow controller. Fig. 6 shows the time course for the total flow rate of the outlet gas in both the retentate and permeate, and the conversion of  $H_2SO_4$  decomposition at 600 °C in a SiC particle-derived membrane reactor. A brief flow sheet with or without extraction is shown in ESI-4.† The membrane reactor with extraction,  $O_2$  with low molecular weight was transferred faster than  $SO_2$  and  $SO_3$ , and  $SO_3$ , and the largest molecular weight, permeated at the slowest speed by Knudsen diffusion through the

mesoporous SiC membrane.<sup>46</sup> Therefore, the equilibrium of the reaction (R4) ( $SO_3 \leftrightarrow SO_2 + 0.5O_2$ ) was forwarded to the product side by removing  $O_2$ . In a comparison with a membrane without extraction, the membrane reactor with extraction achieved higher conversion at the same temperature of 600 °C. The catalytic membrane reactor obtained conversion of 25% without extraction, which approximated the equilibrium (theoretical) conversion of  $SO_3$  decomposition (eqn (4)) of 28% at 900 K.<sup>3</sup> Comparison with membrane without extraction, the conversion of  $H_2SO_4$  decomposition was increased to 45%, which was much higher at the same temperature of 600 °C. Additionally, the  $H_2SO_4$  decomposition conversion remained constant at around 41% after membrane exposure to  $H_2SO_4$  vapor for 10 h. Moreover, after decomposition for 10 h, He permeance was approximately the same as that before the decomposition reaction, which indicated that the SiC particle layer (with  $SiO_2-ZrO_2$ ) had high hydrothermal and chemical stability under  $H_2O$  and  $SO_3$ . However, the separation properties of M4 membranes was still poor; the He/ $N_2$  permeance ratio was 2.3 with  $N_2$  permeance of  $4.5 \times 10^{-5} \text{ mol m}^{-2} \text{ s}^{-1} \text{ Pa}^{-1}$ , since the SiC membrane was fabricated using SiC particles, and the gaps between particles were large enough to allow gas to pass through.

## 4. Conclusions

SiC mesoporous membranes were successfully prepared using an  $\alpha-Al_2O_3$  support and a SiC particle layer. The gas permeance of the SiC membrane was stable for 20 h under  $H_2SO_4$  vapor at 600 °C, which indicated its high chemical stability. Regarding the  $H_2SO_4$  decomposition reaction, the SiC membrane achieved a conversion of 41% at 600 °C, which was much higher than that of the membrane without extraction (25%). Our previous work involved the preliminary use of SiC membranes in a catalytic membrane reactor for hydrogen production in the iodine-sulfur process, and a desirable design for a SiC subnanoporous membrane with a combination of high  $O_2$  permeance and  $O_2/SO_2$  selectivity will be a major objective in the future.

## Conflicts of interest

There are no conflicts to declare.

## Acknowledgements

This work was supported by the Cross-ministerial Strategic Innovation Promotion Program (SIP) of the Energy Carrier Project of the Japan Science and Technology Agency (JST) and the Japan Society for the Promotion of Science (JSPS) KAKENHI Grant Number JP20H052279.

## Notes and references

- 1 S. Kasahara, G.-J. Hwang, H. Nakajima, H.-S. Choi, K. Onuki and M. Nomura, Effects of process parameters of the IS process on total thermal efficiency to produce hydrogen from water, *J. Chem. Eng. Jpn.*, 2003, **36**, 887–899.

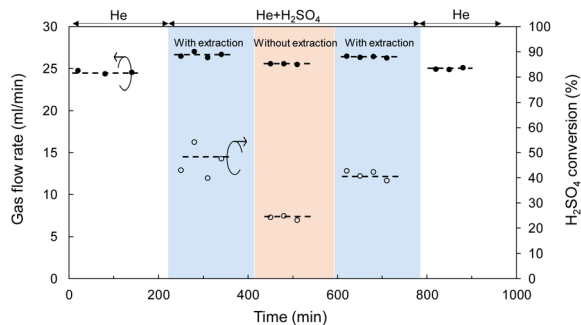


Fig. 6 Time course of gas flow rate and  $H_2SO_4$  conversion for a SiC membrane tested in the catalytic membrane reactor at 600 °C.



- 2 D. M. Ginosar, H. W. Rollins, L. M. Petkovic, K. C. Burch and M. J. Rush, High-temperature sulfuric acid decomposition over complex metal oxide catalysts, *Int. J. Hydrogen Energy*, 2009, **34**, 4065–4073.
- 3 L. Meng, M. Kanezashi and T. Tsuru, Catalytic membrane reactors for SO<sub>3</sub> decomposition in iodine–sulfur thermochemical cycle: a simulation study, *Int. J. Hydrogen Energy*, 2015, **40**, 12687–12696.
- 4 O. Myagmarjav, A. Ikeda, N. Tanaka, S. Kubo and M. Nomura, Preparation of an H<sub>2</sub>-permselective silica membrane for the separation of H<sub>2</sub> from the hydrogen iodide decomposition reaction in the iodine–sulfur process, *Int. J. Hydrogen Energy*, 2017, **42**, 6012–6023.
- 5 X. Yu, L. Meng, H. Nagasawa, M. Kanezashi, M. Machida and T. Tsuru, Evaluating the chemical stability of metal oxides in SO<sub>3</sub> and applications of SiO<sub>2</sub>-based membranes to O<sub>2</sub>/SO<sub>3</sub> separation, *J. Am. Ceram. Soc.*, 2019, **102**, 6946–6956.
- 6 A. Nadar, A. M. Banerjee, M. Pai, S. S. Meena, R. Pai, R. Tewari, S. Yusuf, A. Tripathi and S. Bharadwaj, Nanostructured Fe<sub>2</sub>O<sub>3</sub> dispersed on SiO<sub>2</sub> as catalyst for high temperature sulfuric acid decomposition—structural and morphological modifications on catalytic use and relevance of Fe<sub>2</sub>O<sub>3</sub>–SiO<sub>2</sub> interactions, *Appl. Catal., B*, 2017, **217**, 154–168.
- 7 M. Nomura, Application of an electrochemical membrane reactor to the thermochemical water splitting IS process for hydrogen production, *J. Membr. Sci.*, 2004, **240**, 221–226.
- 8 X. Liu, B. Jiang, X. Yin, H. Ma and B. S. Hsiao, Highly permeable nanofibrous composite microfiltration membranes for removal of nanoparticles and heavy metal ions, *Sep. Purif. Technol.*, 2020, **233**, 115976.
- 9 P. H. Duong, V. A. Kuehl, B. Mastorovich, J. O. Hoberg, B. A. Parkinson and K. D. Li-Oakey, Carboxyl-functionalized covalent organic framework as a two-dimensional nanofiller for mixed-matrix ultrafiltration membranes, *J. Membr. Sci.*, 2019, **574**, 338–348.
- 10 S. Anisah, W. Puthai, M. Kanezashi, H. Nagasawa and T. Tsuru, Preparation, characterization, and evaluation of TiO<sub>2</sub>–ZrO<sub>2</sub> nanofiltration membranes fired at different temperatures, *J. Membr. Sci.*, 2018, **564**, 691–699.
- 11 G. Dong, H. Nagasawa, L. Yu, M. Guo, M. Kanezashi, T. Yoshioka and T. Tsuru, Energy-efficient separation of organic liquids using organosilica membranes via a reverse osmosis route, *J. Membr. Sci.*, 2020, **597**, 117758.
- 12 Y. Ying, M. Tong, S. Ning, S. K. Ravi, S. B. Peh, S. C. Tan, S. J. Pennycook and D. Zhao, Ultrathin Two-Dimensional Membranes Assembled by Ionic Covalent Organic Nanosheets with Reduced Apertures for Gas Separation, *J. Am. Chem. Soc.*, 2020, **142**, 4472–4480.
- 13 C. Z. Liang, T.-S. Chung and J.-Y. Lai, A review of polymeric composite membranes for gas separation and energy production, *Prog. Polym. Sci.*, 2019, **97**, 101141.
- 14 L. Yu, M. Kanezashi, H. Nagasawa, N. Moriyama, T. Tsuru and K. Ito, Enhanced CO<sub>2</sub> separation performance for tertiary amine-silica membranes via thermally induced local liberation of CH<sub>3</sub>Cl, *AIChE J.*, 2018, **64**, 1528–1539.
- 15 X. Ren, M. Kanezashi, H. Nagasawa and T. Tsuru, Plasma-assisted multi-layered coating towards improved gas permeation properties for organosilica membranes, *RSC Adv.*, 2015, **5**, 59837–59844.
- 16 G. Gong, H. Nagasawa, M. Kanezashi and T. Tsuru, Reverse osmosis performance of layered-hybrid membranes consisting of an organosilica separation layer on polymer supports, *J. Membr. Sci.*, 2015, **494**, 104–112.
- 17 T. Tsuru, Silica-Based Membranes with Molecular-Net-Sieving Properties: Development and Applications, *J. Chem. Eng. Jpn.*, 2018, **51**, 713–725.
- 18 M. Elimelech and W. A. Phillip, The future of seawater desalination: energy, technology, and the environment, *Science*, 2011, **333**, 712–717.
- 19 M. Nomura, T. Kodaira, A. Ikeda, Y. Naka, H. Nishijima, S.-i. Imabayashi, S.-i. Sawada, T. Yamaki, N. Tanaka and S. Kubo, Development of ion-exchange membranes for the membrane bunsen reaction in thermochemical hydrogen production by iodine-sulfur process, *J. Chem. Eng. Jpn.*, 2018, **51**, 726–731.
- 20 O. Myagmarjav, J. Iwatsuki, N. Tanaka, H. Noguchi, Y. Kamiji, I. Ioka, S. Kubo, M. Nomura, T. Yamaki and S. Sawada, Research and development on membrane IS process for hydrogen production using solar heat, *Int. J. Hydrogen Energy*, 2019, **44**, 19141–19152.
- 21 O. Myagmarjav, N. Tanaka, M. Nomura and S. Kubo, Module design of silica membrane reactor for hydrogen production via thermochemical IS process, *Int. J. Hydrogen Energy*, 2019, **44**, 10207–10217.
- 22 N. Tanaka, H. Noguchi, Y. Kamiji, H. Takegami and S. Kubo, Hydriodic iodide and iodine permeation characteristics of fluoropolymers as a lining material, *Int. J. Hydrogen Energy*, 2020, **45**, 17557–17561.
- 23 B. Bhushan, N. Goswami, S. Parida, B. Rath, S. A. Kumar, V. Karki, R. Bindal and S. Kar, Corrosion behavior analyses of metallic membranes in hydrogen iodide environment for iodine-sulfur thermochemical cycle of hydrogen production, *Int. J. Hydrogen Energy*, 2018, **43**, 10869–10877.
- 24 B. Huang, Y. Zhu, Y. He, S. Xu, Y. Zhang and Z. Wang, Influence of catalyst coated membranes on electrochemical bunsen reaction in the sulfur-iodine cycle, *Int. J. Hydrogen Energy*, 2019, **44**, 9735–9742.
- 25 C. Forsberg, L. Trowbridge, B. Bischoff and L. K. Mansur, Sulfur thermochemical processes with inorganic membranes to produce hydrogen, *CiteSeer, AIChE Spring National Meeting New Orleans*, Louisiana, USA, 2004.
- 26 G. He, R. H. Elder, D. C. Sinclair and R. W. K. Allen, High temperature oxygen separation for the sulphur family of thermochemical cycles – Part II: sulphur poisoning and membrane performance recovery, *Int. J. Hydrogen Energy*, 2013, **38**, 785–794.
- 27 O. Myagmarjav, N. Tanaka, M. Nomura and S. Kubo, Comparison of experimental and simulation results on catalytic HI decomposition in a silica-based ceramic membrane reactor, *Int. J. Hydrogen Energy*, 2019, **44**, 30832–30839.



- 28 L. Meng, M. Kanezashi, X. Yu and T. Tsuru, Enhanced decomposition of sulfur trioxide in the water-splitting iodine-sulfur process via a catalytic membrane reactor, *J. Mater. Chem. A*, 2016, **4**, 15316–15319.
- 29 M. Elma, C. Yacou, J. C. Diniz da Costa and D. K. Wang, Performance and long term stability of mesoporous silica membranes for desalination, *Membranes*, 2013, **3**, 136–150.
- 30 G. Caputo, C. Felici, P. Tarquini, A. Giaconia and S. Sau, Membrane distillation of HI/H<sub>2</sub>O/H<sub>2</sub>O and H<sub>2</sub>SO<sub>4</sub>/H<sub>2</sub>O<sub>2</sub>SO<sub>4</sub>/H<sub>2</sub>O mixtures for the sulfur-iodine thermochemical process, *Int. J. Hydrogen Energy*, 2007, **32**, 4736–4743.
- 31 H. Schoeman, H. M. Krieg, A. J. Kruger, A. Chromik, K. Krajcinovic and J. Kerres, H<sub>2</sub>SO<sub>4</sub> stability of PBI-blend membranes for SO<sub>2</sub> electrolysis, *Int. J. Hydrogen Energy*, 2012, **37**, 603–614.
- 32 M. Kanezashi, K. Yada, T. Yoshioka and T. Tsuru, Design of silica networks for development of highly permeable hydrogen separation membranes with hydrothermal stability, *J. Am. Chem. Soc.*, 2009, **131**, 414–415.
- 33 X. Yu, H. Nagasawa, M. Kanezashi and T. Tsuru, Improved thermal and oxidation stability of bis(triethoxysilyl)ethane (BTESE)-derived membranes, and their gas-permeation properties, *J. Mater. Chem. A*, 2018, **6**, 23378–23387.
- 34 H. L. Casticum, A. Sah, R. Kreiter, D. H. A. Blank, J. F. Vente and J. E. Ten Elshof, Hydrothermally stable molecular separation membranes from organically linked silica, *J. Mater. Chem.*, 2008, **18**, 2150–2158.
- 35 W. Puthai, M. Kanezashi, H. Nagasawa, K. Wakamura, H. Ohnishi and T. Tsuru, Effect of firing temperature on the water permeability of SiO<sub>2</sub>-ZrO<sub>2</sub> membranes for nanofiltration, *J. Membr. Sci.*, 2016, **497**, 348–356.
- 36 J. Zhang, R. Zhang, X. Chen, M. Tong, W. Kang, S. Guo, Y. Zhou and J. Lu, Simultaneous Removal of NO and SO<sub>2</sub> from Flue Gas by Ozone Oxidation and NaOH Absorption, *Ind. Eng. Chem. Res.*, 2014, **53**, 6450–6456.
- 37 L. Meng, M. Kanezashi, J. Wang and T. Tsuru, Permeation properties of BTESE-TEOS organosilica membranes and application to O<sub>2</sub>/SO<sub>2</sub> gas separation, *J. Membr. Sci.*, 2015, **496**, 211–218.
- 38 A. Nadar, A. M. Banerjee, M. Pai, R. Pai, S. S. Meena, R. Tewari and A. Tripathi, Catalytic properties of dispersed iron oxides Fe<sub>2</sub>O<sub>3</sub>/MO<sub>2</sub> (M= Zr, Ce, Ti and Si) for sulfuric acid decomposition reaction: role of support, *Int. J. Hydrogen Energy*, 2018, **43**, 37–52.
- 39 M. Landau, S. Varkey, M. Herskowitz, O. Regev, S. Pevzner, T. Sen and Z. Luz, Wetting stability of Si-MCM-41 mesoporous material in neutral, acidic and basic aqueous solutions, *Microporous Mesoporous Mater.*, 1999, **33**, 149–163.
- 40 H. Nayeibzadeh, N. Saghatoleslami and M. Tabasizadeh, Application of microwave irradiation for fabrication of sulfated ZrO<sub>2</sub>-Al<sub>2</sub>O<sub>3</sub> nanocomposite via combustion method for esterification reaction: process condition evaluation, *J. Nanostruct. Chem.*, 2019, **9**, 141–152.
- 41 M. Testa, V. La Parola, F. Mesrar, F. Ouanji, M. Kacimi, M. Ziyad and L. Liotta, Use of Zirconium Phosphate-Sulphate as Acid Catalyst for Synthesis of Glycerol-Based Fuel Additives, *Catalysts*, 2019, **9**, 148.
- 42 P. Graf, D. De Vlieger, B. Mojet and L. Lefferts, New insights in reactivity of hydroxyl groups in water gas shift reaction on Pt/ZrO<sub>2</sub>, *J. Catal.*, 2009, **262**, 181–187.
- 43 T. Ishikawa, Y. Kohtoku, K. Kumagawa, T. Yamamura and T. Nagasawa, High-strength alkali-resistant sintered SiC fibre stable to 2,200 °C, *Nature*, 1998, **391**, 773–775.
- 44 S. Tomar, S. Gangwar, K. Kondamudi and S. Upadhyayula, SO<sub>3</sub> decomposition over β-SiC and SiO<sub>2</sub> supported CuFe<sub>2</sub>O<sub>4</sub>: a stability and kinetic study, *Int. J. Hydrogen Energy*, 2020, **45**, 21287–21296.
- 45 H. A. Khan, P. Natarajan and K.-D. Jung, Stabilization of Pt at the inner wall of hollow spherical SiO<sub>2</sub> generated from Pt/hollow spherical SiC for sulfuric acid decomposition, *Appl. Catal., B*, 2018, **231**, 151–160.
- 46 T. Yoshioka, M. Kanezashi and T. Tsuru, Micropore size estimation on gas separation membranes: a study in experimental and molecular dynamics, *AIChE J.*, 2013, **59**, 2179–2194.

